

# RSC Advances



This is an *Accepted Manuscript*, which has been through the Royal Society of Chemistry peer review process and has been accepted for publication.

*Accepted Manuscripts* are published online shortly after acceptance, before technical editing, formatting and proof reading. Using this free service, authors can make their results available to the community, in citable form, before we publish the edited article. This *Accepted Manuscript* will be replaced by the edited, formatted and paginated article as soon as this is available.

You can find more information about *Accepted Manuscripts* in the [Information for Authors](#).

Please note that technical editing may introduce minor changes to the text and/or graphics, which may alter content. The journal's standard [Terms & Conditions](#) and the [Ethical guidelines](#) still apply. In no event shall the Royal Society of Chemistry be held responsible for any errors or omissions in this *Accepted Manuscript* or any consequences arising from the use of any information it contains.



## RSC Advances

## Paper

## Folic acid-conjugated BSA nanocapsule (n-BSA-FA) for cancer targeted radiotherapy and imaging

Received 00th January 20xx,

Sheng Liang,<sup>†,a</sup> Xin Jin,<sup>†,b</sup> Yufei Ma,<sup>a</sup> Jun Guo,<sup>a</sup> Hui Wang<sup>\*a</sup>

Accepted 00th January 20xx

DOI: 10.1039/x0xx00000x

www.rsc.org/

New carrier systems have generated new opportunities to deliver drugs to specific targets. Capitalizing on recent achievements in the area of nanotechnology and nuclear medicine, we sought to develop a radiolabeled nano-drug that could accumulate in tumors via tumor-selective targeted delivery system and could treat the tumors with radionuclide. <sup>125/131</sup>I-labeled nano-drug, [<sup>125/131</sup>I]-n-BSA-FA, was prepared in this paper, with high radiochemical yield and long stability *in vitro*. Pharmacokinetics and biodistribution studies, as well as SPECT/CT imaging of the radiolabeled nanoparticles, [<sup>125</sup>I]-n-BSA-FA, were performed on a mouse model of breast cancer. Accumulation of this drug in tumor peaked at 24 h after injection and was measured to be 11.3 percentage injected dose per gram (ID%/g). In addition, a therapeutic study was performed to evaluate the therapeutic effect of [<sup>131</sup>I]-n-BSA-FA. It completely retarded the tumor growth with only one injection. The nano-carrier drugs described here targeted malignant tumors and may be useful for both tumor imaging and tumor treatment combined in clinic.

### Introduction

Radiotherapy is an important clinical therapeutic modality for a wide variety of cancers. However, the low therapeutic efficacy limits its clinical applications. The effectiveness of a radio-therapeutic agent for cancer, as represented by therapeutic efficiency, reflects its ability to reduce and eliminate tumors without harming the healthy tissue nearby. The efficiency for a given agent depends on its adequate local delivery to the tumor site. Therefore, target-selective drug delivery with high efficiency, low toxicity, and minimal side effects, is desirable to improve the efficacy of radiotherapeutics. Targeted delivery system should achieve desired organ distribution of radiopharmaceuticals, to enhance tumor specificity.

Recently, application of nanotechnology in the field of tumor treatment became a hot spot.<sup>1,2</sup> Nanocarrier drugs with specific targeting capacity could be non-toxic and biodegradable, and their release could be controllable.<sup>3-6</sup> Several tumor-selective targeted radio-carriers have been successfully constructed with target ligands, such as RGD, folic acid and so on, but achieved limited success as therapeutics. In most cases, the radiopharmaceuticals cannot survive from the clearance of liver, spleen and kidney, while nanoparticles above 8 nm

diameters cannot infiltrate through kidney.<sup>7</sup>

We adapt the strategy to design targeted nano-carrier with proper size that can escape MPS (mononuclear phagocyte system). This, in turn, would make the nanocarriers remain longer in plasma, thus provide more opportunities for the carriers to target tumor. Our previous research showed that reducing surface charge and increasing hydrophobicity were also effective strategies to avoid MPS recognition and clearance<sup>8,9</sup>. Non-fouling polymer pMPC (poly 2-methacryloyloxyethyl phosphorylcholine) is a perfect choice for surface protection.

We select folate as target ligand. Folate receptors express at relatively low levels in most normal cells, but they overexpress at the surface in many kinds of tumor cells. The folate receptors provide a highly selective mechanism to distinguish tumor cells from normal cells.<sup>10-12</sup> Folic acid (FA) has a benign affinity for cell surface receptors.<sup>13</sup> So far folic acid functionalized nanoparticles and nanocarriers have been reported previously in both imaging and therapeutic applications.<sup>14-21</sup>

In this paper, we report a novel radionuclide nano-carrier, which shows long plasma circulation time and high tumor selectivity. In our design of the nanocarrier, three components are constructed as three layers (Figure 1A), which we designated as cargo, pMPC, and folate. BSA (Bovine serum albumin) acts as the stable cargo that has various residues for radiolabelling, such as amide and tyrosine. pMPC encapsulates BSA as the non-fouling layer that can help the nanocarrier to survive from MPS clearance. Folic acid is attached on the nano-carrier surface as tumor selective targeting ligand.

<sup>a</sup> Department of Nuclear Medicine, Xinhua Hospital, School of Medicine, Shanghai Jiaotong University, 1665 Kongjiang Rd., Shanghai 200092, China.

<sup>b</sup> School of Chemistry & Chemical Engineering, Shanghai Jiaotong University, 800 Dongchuan Rd., Shanghai 200240, China.

† These authors contributed equally to this work.

Electronic Supplementary Information (ESI) available: [details of any supplementary information available should be included here]. See DOI: 10.1039/x0xx00000x

## Materials and methods

### Materials

All of the reagents were purchased from Sigma-Aldrich (USA), and were used as received without further purification. The [ $^{125/131}$ ]NaI was purchased from HTA CO. LTD (China). Radioactivity was detected by a CRC-25R Dose Calibrator (Capintec, USA). Thin-layer chromatography (TLC) (Mini Bioscan, USA) was carried out using pre-coated aluminum-backed silica gel 60 GF<sub>254</sub> TLC plates (E. Merk Company, Germany). Female BALB/c nude mice (4–5 weeks of age, 18–20 g) were purchased from the Slaccas Animal Laboratory (Shanghai, China).

### Fluorescence-labeling of BSA

For the imaging purposes, BSA was labeled with fluorescence dye (FITC). Briefly, BSA was firstly dissolved in water and dialyzed against sodium carbonate buffer (20 mM, pH 8.5) to remove any ammonium sulfate that usually exists in the stock protein powder. After dialysis, the protein was diluted to 10 mg/ml with sodium carbonate buffer (20 mM, pH 8.5). Fluorescence isothiocyanate (FITC) was dissolved in DMSO to make a 1% (m/v) stock solution. Then FITC stock solution was added into the protein solution at a molar ratio of 5:1 (Dye:Protein). The reaction mixture was kept at 4°C overnight; the as-formed sample was dialyzed against sodium carbonate buffer (20 mM, pH 8.5) to remove the unconjugated dye.

### Acryloylation of BSA

BSA, or FITC labeled BSA, was firstly conjugated with N-acryloylsuccinimide (NAS) to attach acryloyl groups onto the surface of the protein. A typical procedure is described below. BSA (~ 10 mg/mL) was firstly dialyzed against sodium carbonate buffer (20 mM, pH 8.5) to remove any ammonium sulfate that usually exists in the stock protein powder. After the dialysis, protein solution was diluted to 5 mg/mL with sodium carbonate buffer (20 mM, pH 8.5), followed by adding NAS solution (10% in DMSO, m/v) to perform the conjugation. The amount of NAS used was at 20:1 molar ratio (NAS to protein), and the conjugation was achieved by keeping the reaction at 4°C for 1 h. The solution was then thoroughly dialyzed against pH 7.0 phosphate buffer (20 mM) with a dialysis tubing membrane (MWCO = 10 kDa, Sigma-Aldrich) to remove any unreacted NAS. Acryloylated protein solutions were stored at 4°C for further use.

### Synthesis of positively charged nBSA(+)

After acryloylation, BSA was encapsulated with pMPC, using an in situ polymerization method. 2-methacryloyloxyethyl phosphorylcholine (MPC) and bis-methacrylamide (BIS) were first prepared as 10% (m/v) stock solution in DI-water and anhydrous DMSO, respectively. Then MPC and BIS were added into the solution of the protein being encapsulated with a specific molar ratio (3000:400:1=MPC:BIS:BSA). Additionally, N-(3-Aminopropyl) methacrylamide hydrochloride (APm) was used with a molar ratio of 1:400 (BSA:APm) in the polymerization step to introduce amino-group. The final BSA concentration was tuned

to 1 mg/mL by diluting with phosphate buffer (50mM, pH 7.0). Polymerization was initiated by the addition of ammonium persulfate (APS) and tetramethylethylenediamine (TEMED) and the reaction solution was kept at 4°C for 2 h. After the polymerization, the solution was dialyzed against PBS to remove all unreacted monomers and by-products of small molecules.

### Surface modification by folic acid (FA)

Folic acid was attached onto nBSA through amidation with amino-groups on nBSA(+). Briefly, folic acid was prepared as 1% (m/v) stock solution in sodium carbonate buffer (20 mM, pH 8.5). Folic acid stock solution was added into nBSA(+) solution with a molar ratio 800:1 (FA:BSA). NHS and EDC were added to achieve high efficiency of amidation with a molar ratio of 1:1.5:20 (FA:NHS:EDC). The reaction mixture was kept at 4°C for 2 h in darkness to form nBSA-FA. After the reaction, the solution was dialyzed against PBS to remove all unreacted reagents and by products of small molecules. The amount of folic acid on surface was determined to be 390:1 (M/M, FA protein), by UV VIS spectrophotometry. The size distribution of the nanocarrier was determined to follow a normal distribution, with mean diameter of 20 nm (Figure 1B), by dynamic laser scattering (DLS) and transmission electron microscope (TEM).

### Radio-label nanoparticle by $^{125/131}$ I

Iodination of n-BSA-FA was performed by the Iodogen method. Briefly, 2–10  $\mu$ L [ $^{125/131}$ ]NaI and 20  $\mu$ L nanoparticles were added to a pre-coated tube. The tube was kept in incubation at 37°C for 10 min. The radiolabeled nano-particles were purified using a filter column. At last, the nanocarriers were suspended in PBS and ready for further use.

### Stability in vitro

[ $^{125}$ ]I-n-BSA-FA was mixed with serum from a new-born calf or phosphate buffered saline (PBS, 0.05 M, pH 7.4) for stability test. The mixture was incubated at 37°C or room temperature (RT) for a total of 7 days. The stability was determined at various time points (0, 3h, 12h, 24h, 2d, 3d and 7d) by TLC.

### Cell Lines and Animal Models

The MDA-MB-231 human breast cancer cells and lung cancer cells A549 were obtained from the American Type Culture Collection (ATCC, Manassas, VA) and maintained under standard conditions according to ATCC. All animal experiments were done in accordance with protocols approved by the Institutional Animal Care and Use Committee of Shanghai Jiaotong University.

The MDA-MB-231 tumor model was established by orthotopic injections of  $5 \times 10^6$  cells into the right mammary fat pad of female athymic nude mice. The mice were subjected to micro SPECT/CT studies and biodistribution experiments when the tumor volume reached 100–200 mm<sup>3</sup> (2–3 weeks after implant).

### Cell Uptake and Efflux Studies

Cell uptake studies were performed according to the following protocol. MDA-MB-231 cells and A549 cells were

seeded into 12-well plates at a density of  $5 \times 10^5$  cells/well and incubated overnight. Cells were rinsed three times with PBS, [ $^{125}\text{I}$ ]I-nBSA-FA was added to the culture wells in triplicate (0.3  $\mu\text{Ci}$ /well). After incubating at 37 °C for 0 min, 5 min, 15 min, 30 min, 60 min, 120 min, 240 min, cells were rinsed three times with PBS and lysed with NaOH-SDS (sodium dodecyl sulfate; 0.2 M NaOH, 1 % SDS). The cell lysate was collected into measurement tubes and measured by a  $\gamma$ -counter (Wallac Wizard 2480, PerkinElmer Inc.).

For cell efflux experiment, MDA-MB-231 cells were seeded into 12-well plates at a density of  $5 \times 10^5$  cells/well and incubated overnight. Cells were rinsed three times with PBS; [ $^{125}\text{I}$ ]I-nBSA-FA was added to the culture wells in triplicate (0.3  $\mu\text{Ci}$ /well). After incubation at 37 °C for 2 h, the cells were washed with PBS, and then re-incubated with serum-free medium. At six different time points (0 min, 15 min, 30 min, 60 min, 120 min, 240 min, 360 min), the cells were washed with PBS and lysed with NaOH-SDS. The cell lysate was collected into measurement tubes for counting. The cell uptake and efflux values were normalized to the amount of added radioactivity for each well.

#### Pharmacokinetics

Five BALB/c mice, each weighing approximately 20 g, were all injected with 0.2 mCi of [ $^{125}\text{I}$ ]I-n-BSA-FA each through the lateral tail vein. Blood samples were withdrawn through the lateral tail vein at several time points from 1 h to 120 h. The blood samples were weighed and radioactivity was counted together with a standard [ $^{125}\text{I}$ ]I-n-BSA-FA solution prepared at the time of injection. The percentage of injected dose per gram of blood (%ID/g) was plotted as the function of time.

#### In Vivo Imaging and Ex Vivo Biodistribution

In vivo imaging was performed and analyzed using a Nano-SPECT/CT (Bioscan, USA). [ $^{125}\text{I}$ ]I-n-BSA-FA (100  $\mu\text{L}$  in PBS, 1 mCi) was injected intravenously into a breast tumor-bearing mouse via the tail vein, and the imaging was performed at 3 h, 1 d, 7 d and 15 d after the injection ( $n=3$  per group). During the injection and image acquisition process, the mice were anesthetized with 2.5% isoflurane in oxygen delivered at a flow rate of 1.5 L/min. FA (10 mg/kg) was injected 30 min prior to injection of [ $^{125}\text{I}$ ]I-n-BSA-FA, to eliminate the variation of FA within each animal. All images were normalized and analyzed using VivoScope software (Bioscan, USA). For quantitative comparison, regions of interest (ROI) were drawn over tumors and muscle, and the average signal for each area was measured.

For the ex vivo biodistribution study, mice were sacrificed at different time point after the injection of [ $^{131}\text{I}$ ]NaI, [ $^{131}\text{I}$ ]I-n-BSA and [ $^{131}\text{I}$ ]I-n-BSA-FA, respectively, and tumor tissues and major organs were carefully harvested. All samples were rinsed with saline, placed into tubes, and immediately counted using  $\gamma$ -counting. For quantitative comparison, ROIs were calculated as described above.

#### Therapeutic study

The animal model used for therapy studies was the same as that described above for the imaging studies. At 4 weeks post implant, animals were randomly divided into four groups ( $n=4$  for each group). The G1 group (control group) was injected with saline. The G2 group ([ $^{131}\text{I}$ ]NaI only group) was injected with 0.5 mCi [ $^{131}\text{I}$ ]NaI. The G3 group ([ $^{131}\text{I}$ ]I-n-BSA group) was injected with 0.5 mCi [ $^{131}\text{I}$ ]I-n-BSA. The G4 group (treatment group) was injected with 0.5 mCi [ $^{131}\text{I}$ ]I-n-BSA-FA each via a lateral tail vein. The mice received food and water ad libitum, and the mice weighed on the day of radioligand administration and every week thereafter. The tumor dimensions were determined with a caliper without the identity of mice and the volumes of the tumor were calculated using the formula for an ellipsoid  $V = \pi/6(d_1 \times d_2 \times d_3)$ , where  $d_1$ ,  $d_2$  and  $d_3$  represent the three largest diameters of the hypothetical ellipsoid. Tumor volumes were normalized and expressed as equivalents of their initial volumes. This procedure was chosen because of the differences in the size of the tumor at the start of the study, and in the multiplicity of tumors in a single animal. Tumor necrosis and loss of more than 10% of original body weight were an indication to sacrifice the mice.

## Results and discussion

### Synthesis of functional nanoparticle

Our design of the nanocarrier drug consists of 3 layers, a single BSA protein core, non-fouling pMPC outer shell, and folic acid as target ligand on the surface (Figure 1A). BSA was selected based on its spherical shape and availability of functional groups to attach radionuclides. Non-fouling polymer layer was chosen to optimize *in vivo* distribution of the nano-carrier. Folic acid was selected to endow high and effective tumor selective target ability.

This synthesis of the nanocarrier was achieved in 2 stages, *in situ* co-polymerization with the protein and surface modification on the nano-particles. Argorose gel analysis showed the formation of nanoparticles with molecular weight much larger than original BSA. DLS and TEM results showed that n-BSA-FA has a uniformed morphology: a spherical nanoparticle with diameter around 20 nm (Figure 1B). By considering the size of BSA at the core and hydrophobicity of MPC, it is reasonable to conclude that n-BSA-FA has only single protein core inside. In order to gain a neutral zeta potential for n-BSA-FA, the amount of FA (folic acid) attached to the surface was controlled within a narrow range of 20%.

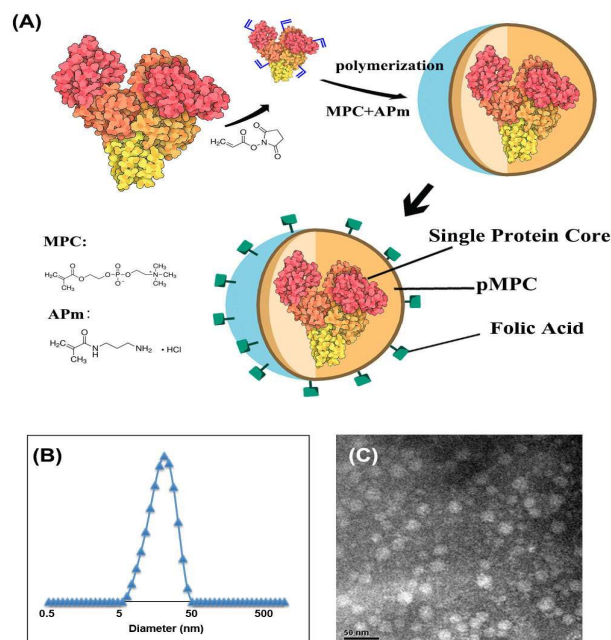


**Figure 1.** Cartoon illustration of n-BSA-FA. A) Synthesis route and structure sketch of n-BSA-FA; B) hydrodynamic diameter of n-BSA-FA of around 20 nm from DLS; C) Transmission electron micrograph of n-BSA-FA with uniform size distribution, negatively dyed by PTA.

### Radiochemistry and in vitro stability

$^{125/131}\text{I}$  radioisotope was chosen for its life-time for imaging, its released energy for therapeutics, and its convenient introduction into protein for radiolabeling. TLC analysis of the synthesized  $[\text{}^{125/131}\text{I}]\text{-n-BSA-FA}$  showed its radiochemical purity >98% after purification by size-exclusion chromatography. Specific activities for  $[\text{}^{125}\text{I}]\text{-n-BSA-FA}$  ranged from 120 to 150 MBq/mg (mean, 140 MBq/mg).

The radiotracer was stable for about 3 h, at the beginning of the experiments (Figure 2). From 12 hours on, the  $[\text{}^{125}\text{I}]\text{-n-BSA-FA}$  decomposed quickly, especially in new-born calf serum. The radiochemistry purity of the nanocarrier was  $75.76 \pm 2.04\%$ , and  $52.94 \pm 1.97\%$  after 3 days. The results showed that this nanocarrier was more stable in PBS than in new-born calf serum at all of the time points, probably from protein-assisted decomposition.

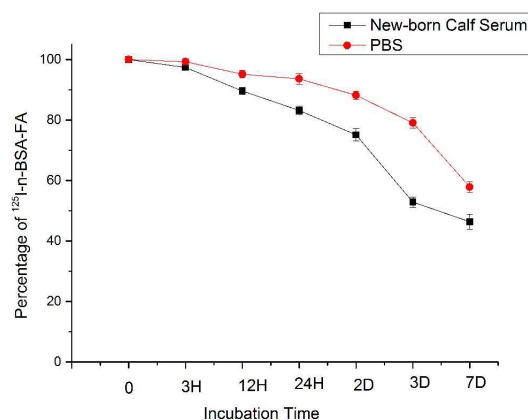


**Figure 2.** The stability of  $[\text{}^{125}\text{I}]\text{-n-BSA-FA}$  in vitro

### Cellular Uptake and Efflux Study

The cellular uptake of  $[\text{}^{125}\text{I}]\text{-n-BSA-FA}$  and  $[\text{}^{125}\text{I}]\text{-FA}$  were evaluated in both MDA-MB-231 cells, which highly express folic acid receptor, and A549 cells, which have a low expression of folic acid receptor.<sup>22</sup> As expected, the uptake of both  $[\text{}^{125}\text{I}]\text{-n-BSA-FA}$  and  $[\text{}^{125}\text{I}]\text{-FA}$  were high in the MDA-MB-231 cells (Figure 3).  $[\text{}^{125}\text{I}]\text{-n-BSA-FA}$  had higher uptake than  $[\text{}^{125}\text{I}]\text{-FA}$  at all of the time points. In contrast, both  $[\text{}^{125}\text{I}]\text{-n-BSA-FA}$  and  $[\text{}^{125}\text{I}]\text{-FA}$  had low uptake in A549 cells.

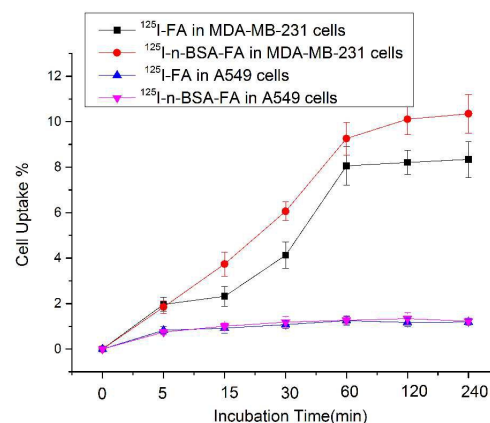


**Figure 3.** Cell uptake assay of  $[\text{}^{125}\text{I}]\text{-n-BSA-FA}$  and  $[\text{}^{125}\text{I}]\text{-FA}$  in MDA-MB-231 cells or A549 cells ( $n=3$ , mean $\pm$ SD).

### Pharmacokinetics

The clearance rate of  $[\text{}^{125}\text{I}]\text{-n-BSA-FA}$  radioactivity in blood-time was slow (Figure 4), with  $1.52 \pm 0.12\%$  ID/g after 3 days, and  $1.13 \pm 0.1\%$  ID/g after 7 days. The radioactivity level for the first 3 days was almost constant at a high level under the experimental conditions. This result confirmed our previous results that reducing surface charge and increasing hydrophobicity were effective to reduce the MPS recognition and clearance. The non-fouling polymer layer we used here not only has the capacity to evade the mononuclear phagocyte

system (MPS) better but also has substantially lower liver and spleen uptake after injection. We believe that MPS system recognizes foreign component through electrostatic interaction at first, and non-fouling polymer layer encapsulates the protein core so nicely and tightly that the neutralized outer layer cannot be recognized and cleared by MPS system.

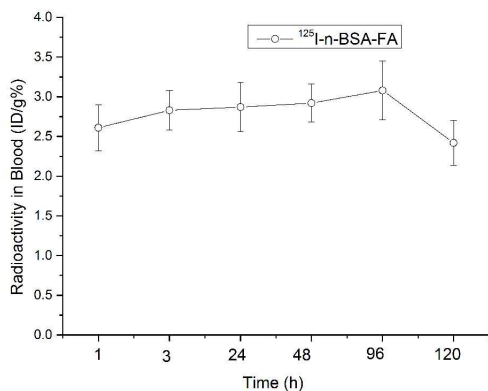


Figure 4. [<sup>125</sup>I]-n-BSA-FA radioactivity in blood-time curve (n=5)

### Biodistribution studies

A dramatically higher distribution in tumor site for [<sup>125</sup>I]-n-BSA-FA was observed, compared with that of [<sup>125</sup>I]NaI, or [<sup>125</sup>I]-n-BSA (without target ligand), in tumor-bearing mice, supporting the tumor-targeting ability and efficiency of the nano-carrier (Figure 5B). The radioactivity uptake in tumor grafts was  $7.66 \pm 0.43$  %ID/g as early as 1 d after injection, and remained consistently high of  $2.29 \pm 0.19$  %ID/g 7 d after injection, demonstrating retention effect of the Folic-targeted nanoparticles. In addition, the nano-particle accumulated in tumor in higher rate. The tumor-to-blood uptake ratios were 1.06, 1.52, 3.11 at 3 d for [<sup>125</sup>I]NaI, [<sup>125</sup>I]-n-BSA and [<sup>125</sup>I]-n-BSA-FA, respectively.

The nano-carriers, n-BSA and n-BSA-FA, showed higher concentration of radioactivity <sup>125</sup>I circulating in plasma than free [<sup>125</sup>I]NaI, in terms of ID/g in blood (Figure 5B). The blood-pool radioactivity was  $3.67 \pm 0.35$  percentage injected dose per gram (%ID/g) at 1 d and slowly decreased to  $1.13 \pm 0.1$  %ID/g on 7 d, slower washout compared with other organs.

As an indication of radioiodine metabolism, thyroid uptake was also assessed over time. No dependence of thyroid uptake on carriers was observed after injection (Figure 5B). Thyroid levels ranged from  $14.96 \pm 1.01$  %ID/g at 1 d to  $6.99 \pm 0.51$  %ID/g at 7 d for [<sup>125</sup>I]-n-BSA-FA;  $15.59 \pm 1.33$  %ID/g,  $6.03 \pm 0.53$  %ID/g for [<sup>125</sup>I]NaI group, and  $16.73 \pm 1.58$  %ID/g,  $7.35 \pm 0.64$  %ID/g for [<sup>125</sup>I]-n-BSA group. Except for tumor and blood, no significant change in uptake of radioactivity in other organs was observed among the 3 radioactive agents evaluated here. The absorption in liver and spleen was  $4.87 \pm 0.39$  %ID/g,  $4.26 \pm 0.32$  %ID/g for [<sup>125</sup>I]-n-BSA-FA; and  $4.68 \pm 0.52$  %ID/g,  $4.21 \pm 0.39$  %ID/g for [<sup>125</sup>I]-n-BSA at 1 d after injection.

### SPECT/CT Imaging Studies

SPECT/CT imaging showed an intense and persistent signal of tumor in all times during four weeks period of observation. The distribution of [<sup>125/131</sup>I]-n-BSA-FA in tumor was homogenous (Figure 5A).

In vivo micro SPECT imaging confirms the tumor location and volume at the left flank of the mice bearing subcutaneous tumor grafts (Figure 5A). After single injection, n-BSA-FA circulates in body for days and has reasonable distribution in major organs, but mainly in heart. Different from normal nanoparticles, n-BSA-FA showed no abnormal distribution in liver and spleen, indicating that the neutral polymer layer helps the nano-carrier to escape MPS recognition and clearance.

The time course of in vivo micro SPECT imaging matches the design expectation of n-BSA-FA with strong tumor-targeting ability (Figure 5A). The relative ratio of the radioactivity in tumor continued to increase post injection of the radioactivity, indicating that n-BSA-FA continues to accumulate in tumor site. One week after injection, when radioactivity has been mostly cleared in other organs, significant radioactivity intensity still remained at the tumor site. The SPECT signal could still be observed 28 days post-injection, although the relative signal intensity has reduced because of the abnormal growth of tumor during that period. The long-time tumor-specific distribution and retention of n-BSA-FA may suggest its potential use as a promising tumor-targeting nano-carrier.

Strong SPECT signal in bladder may suggest the metabolism pathway of n-BSA-FA be through kidney and excrete through urine (Figure 5A and 5B).

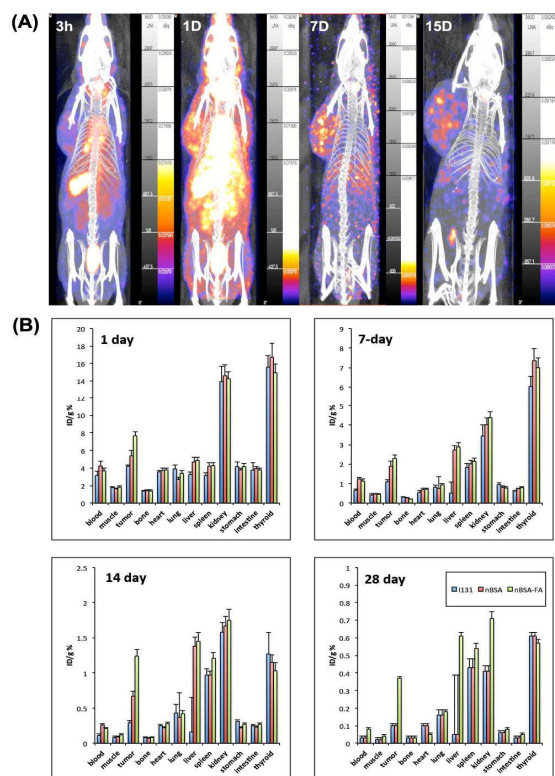


**Figure 5.** Biodistribution of n-BSA-FA (A) SPET-CT images of tumor mice after injection of  $^{131}\text{I}$  labeled n-BSA-FA ( $^{131}\text{I}$ -nBSA-FA) of 3 hour, one day, seven days and fifteen days (B) Biodistribution of  $^{131}\text{I}$ -n-BSA-FA in organs with one day, seven days, fourteen days and twenty-eight days post-injection, separately.

### Therapeutic study

The therapeutic effect of 3 radiolabeled agents were evaluated and compared, including  $^{131}\text{I}$ NaI,  $^{131}\text{I}$ -n-BSA, and  $^{131}\text{I}$ -n-BSA-FA. As described above, the nanocarrier showed long circulation in blood, as well as long time retention in tumor, so all tumor-bearing mice received only one injection of radioisotope treatment.  $^{131}\text{I}$  was chosen as model therapeutic radioactive labeling to form the anticancer nano-drug. n-BSA was also labeled with  $^{131}\text{I}$  to illustrate the anticancer effect of non-targeted nano-drug. The tumor treated with saline progressed rapidly; while tumors treated by free  $^{131}\text{I}$ NaI or  $^{131}\text{I}$ -n-BSA progressed in a much slower rate. Tumors in n-BSA-FA-treated group progressed in the same rate as  $^{131}\text{I}$ NaI and  $^{131}\text{I}$ -n-BSA-treated groups at the initial 7 days. However, the tumor growth was completely retarded during the following observation, where tumor volume remained almost at the same size at 23th day as at 7th day (Figure 6A). 7 days post injection, the tumor sizes no longer changed at the n-BSA-FA-treated group. The retarding effect sustained for the following 16 days, until the completion of the whole experiment. The tumor growth at the  $^{131}\text{I}$ NaI and  $^{131}\text{I}$ -n-BSA treated groups was also lower than that of the control group, where no radioactivity was injected. This may come from the

accumulation of radioactivity in the breast cancer cells by the circulation of the radioactivity in blood, but, without targeting agent, the radioactivity could not stay for a long time. The anticancer effect of  $^{131}\text{I}$ NaI and  $^{131}\text{I}$ -n-BSA was limited.

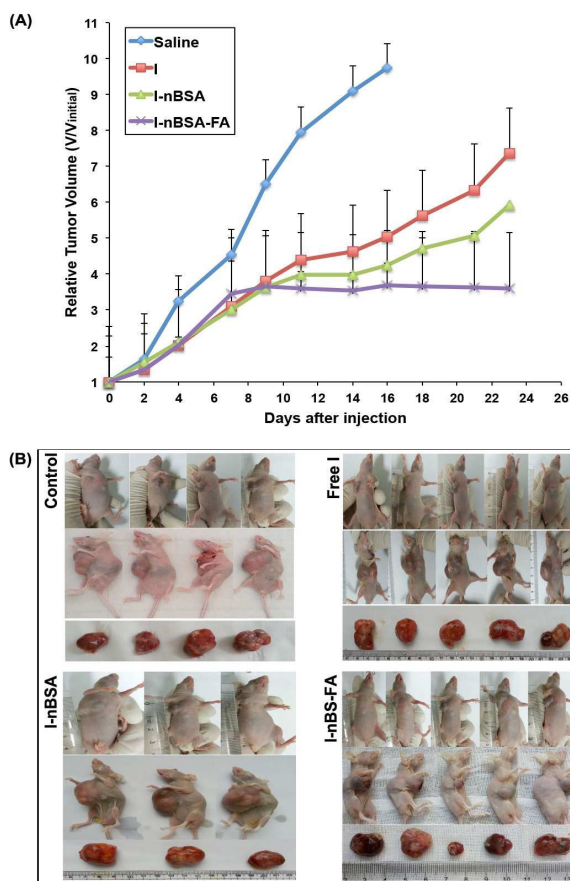


**Figure 6.** Anticancer effect of nano-carriers: (A) Tumor volume change after single injection of saline,  $^{131}\text{I}$ NaI,  $^{131}\text{I}$ -nBSA and  $^{131}\text{I}$ -nBSA-FA; (B) Photo illustration of tumors before and after single injection treatment.

Except for the active targeting effect observed for  $^{131}\text{I}$ -n-BSA-FA, we also observed passive size-determined diffusion (enhanced permeability and retention effect, EPR). This is manifested in the higher anticancer effect of  $^{131}\text{I}$ -n-BSA as compared to that of  $^{131}\text{I}$ NaI. This EPR effect could also have significant contribution of the therapeutic effect of  $^{131}\text{I}$ -n-BSA-FA, which completely retarded the tumor growth with only one injection. In summary, the anticancer effect of the nanodrug,  $^{131}\text{I}$ -n-BSA-FA, comes from active targeting effect, which stems from the combination of pMPC protective layer and folic acid as target ligand, and passive diffusion effect from the nanoparticle size. The former effect makes the nanodrug to have long plasma retention time and to have targeting ability toward cancer cells overexpressing FA-receptors. The latter effect makes the nanodrug stay longer and accumulate faster at the tumor site.  $^{131}\text{I}$ -n-BSA-FA has potential as radioactive nano-drug.

## Conclusions

In this study, we present the synthesis and evaluation of [ $^{125/131}$ I]-labeled nano-particles. The resulting nano-drug, [ $^{131}$ I]-n-BSA-FA, showed long-circulation in blood, and targeted selectively the cancer cell overexpressing FA-receptors both in vitro and in vivo. The nano-drug, [ $^{125/131}$ I]-n-BSA-FA, can be used as imaging agent in SPECT imaging [ $^{125}$ I]-n-BSA-FA, and used as therapeutic agent to inhibit tumor growth [ $^{131}$ I]-n-BSA-FA with only one injection. We believe that the nanodrug described here could be adapted for other nanoparticles with different targets.

## Acknowledgements

We thank National Natural Science Foundation of China (51343007) for financial support.

## Notes and references

- 1 V. P. Torchilin. *Advanced Drug Delivery Reviews*, 2006, 58(24), 1532-1555.
- 2 B. Halye, and E. Frenkel, *Urologic Oncology: Seminars and Original Investigations*, 2008, 26 (1), 57-64.
- 3 A. Beduneau, P. Saulnier and J. P. Benoit, *Biomaterials*, 2007, 28(33), 4947-4967.
- 4 P. R. Lockman, R. J. Mumper, M. A. Khan and D. D. Allen, *Drug. Dev. Ind. Pharm.*, 2002, 28(1), 1-13.
- 5 R. Sinha, G. J. Kim, S. Nie and D. M. Shin, *Mol. Cancer. Ther.*, 2006, 5(8), 1909-1917.
- 6 D. Peer, J. M. Karp, S. Hong, O. C. Farokhzad, R. Margalit and R. Langer, *Nature Nanotechnology.*, 2007, 2, 751-760.
- 7 S. Mitragotri and J. Lahann. *Nat. Mater.*, 2009, 8, 15-23.
- 8 Z Chao, S jiang, *Nano Today*, 2014, 7, 404-413.
- 9 Q Shao, L Ma, X Han, T Bai, S Liu, Y Li, S Jiang, *Journal of Physical Chemistry B* 2014, 118, 6956-6962
- 10 J. Sudimack and R. J. Lee, *Adv. Drug. Deliv. Rev.*, 2000, 41, 147-162.
- 11 A. Gabizon, T. Horowitz, D. Goren, D. Tzemach, F. Mandelbaum-Shavit, M. M. Qazen and S. Zalipsky, *Bioconjugate. Chem.*, 1999, 10, 289-298.
- 12 L Xu, KF Pirolo, EH Chang. *J Controlled Release*, 2001, 74, 115-128.
- 13 Y. Lu and P. S. Low, *Adv. Drug. Deliv. Rev.*, 2002, 54, 675-693.
- 14 S. W. Tsai, J. W. Liaw, F. Y. Hsu, C, T, Yun, L. M. Jhih and Y. M. His, *Sensors*, 2008, 8, 6660-6673.
- 15 Y. Teow and S. Valiyaveetil, *Nanoscale*, 2010, 2, 2607-2613.
- 16 M. Geszke, M. Muris, L. Balan, G. Medjahdi, J. Korczynski, M. Moritz, J. Lulek, R. Schneider, *Acta Biomaterialia*, 2011, 7, 1327-1338.
- 17 C. Sun, R. Sze, M. Zhang, *J. Biomedical Materials Research, Part A*, 2006, 78A, 550-557.
- 18 B. Stella, S. Arpicco, M. T. Peracchia, D. Desmaele, J. Hoebeke, M. Renoir, J. D'angelo, L. Cattel, P. Couvreur, *J. Pharmaceutical Sciences*, 2000, 89, 1452-1464.
- 19 S. Wang, P. S. Low, *J. Controlled Release*, 1998, 53, 39-48.
- 20 P. Huang, L. Bao, C. Zhang, J. Lin, T. Luo, D. Yang, M. He, Z. Li, G. Gao, B. Gao, S. Fu, D. Cui, *Biomaterials*, 2011, 32, 9796-9809.
- 21 Y. Bae, N. Nishiyama, K. Kataoka, *Bioconjugate Chem*, 2007, 18, 1131-1139.

22 Y. Li, R. Chen, Y. Y. Li, K. Sharafudeen, S. J. Liu, D. K. Wu, Y. L. Qin, J. R. Qiu, *Microchimica Acta*, 2015, 182, 1827-1834.